Precise ^{92}Rb and ^{96}Y yields for thermal-neutron-induced fission of ^{235}U and ^{239,241}Pu determined using calorimetric low-temperature detectors

Santwana Dubey [1,2] Artur Echler,[1,2] Peter Egelhof,[1,2] Patrick Grabitz,[1,2] Werner Lauterfeld,[1,2] Manfred Mutterer,[1,2,*]
Stefan Stolte,[1,2] Aurelien Blanc,[3] Ulli Köster,[3] Olivier Serot,[4] Gregoire Kessedjian,[4,5]
Saskia Kraft-Bermuth,[6] Pascal Scholz,[6] and Friedrich Gönnenwein[7]

[1]*Johannes Gutenberg Universität, Mainz, Germany*
[2]*GSI Helmholtzzentrum für Schwerionenforschung, Darmstadt, Germany*
[3]*Insitut Laue Langevin, Grenoble, France*
[4]*CEA/DES/IRESNE/DER/SPRC, Cadarache, France*
[5]*LPSC, Université Grenoble-Alpes, CNRS/IN2P3, Grenoble, France*
[6]*Justus Liebig Universität, Giessen, Germany*
[7]*Eberhard Karl Universität, Tübingen, Germany*

The novel technology of calorimetric low-temperature detectors (CLTDs) was applied to determine isotopic yields of fission fragments using the passive absorber method for thermal-neutron-induced fission reactions at the LOHENGRIN mass spectrometer at the Institut Laue-Langevin in Grenoble, France. Precise yields were determined for ^{92}Rb and ^{96}Y. These fission products are the dominant contributors to the high-energy portion of the reactor antineutrino spectra. Our new measurements resolve inconsistencies between previous yield measurements and fission data libraries and reduce the nuclear data uncertainties in the computation of reactor antineutrino spectra by the summation method.

I. INTRODUCTION

The so-called *reactor antineutrino anomaly* [1], an apparent $\approx 2.5\sigma$ deficit in antineutrino rate, has been derived by comparing measured antineutrino rates from nuclear reactors with those computed from integral fission product beta spectra measured previously by Schreckenbach *et al.* with the BILL spectrometer at the Institut Laue-Langevin (ILL) [2–5]. The discrepancy is particularly pronounced for antineutrinos in the energy range from 4 to 6 MeV [6–8]. The observed reactor antineutrino anomaly could either have a particle physics explanation, namely, the existence of a fourth "sterile neutrino" [1], or a nuclear physics explanation, namely, a problem in the conversion of beta to antineutrino spectra. Independently, from a conversion of integral beta spectra, the expected antineutrino spectra can also be computed by the summation method where the contributions of all known decay branches of fission fragments are summed weighted with their fission yields [9–11]. Only a few fission products with very high Q value for beta decay contribute to the high-energy part of the antineutrino spectra. The two main contributors are ^{92}Rb

and ^{96g}Y [11,12]. Vigorous efforts of the neutrino community are ongoing to accurately measure reactor antineutrino spectra at short distances [13–17]. Complementary effort is required for nuclear physics experiments, evaluation, and theory to improve the knowledge of the beta spectra of the key contributors and to reduce uncertainties on their fission yields. The former data are obtained by measurements with total absorption γ-ray spectrometers [18–21], while consistency checks of nuclear data libraries already allowed us to identify and eliminate certain artifacts [22]. We report in the following on new measurements of the fission yields of the two key contributors ^{92}Rb and ^{96g}Y, the former measurement explicitly requested by Dwyer and Langford [12]. Particular effort was devoted to the measurement in thermal-neutron-induced fission of ^{235}U since these results are relevant for the STEREO [13] and PROSPECT [14] experiments which measure at research reactors with pure ^{235}U core. Moreover, the yields were determined for ^{239}Pu and ^{241}Pu, which are additional contributions in power reactors, thus affecting the antineutrino spectra studied by the Double Chooz [23], RENO [6,15], Daya Bay [7,16], and NEOS [17] Collaborations. Precise yield measurements for ^{92}Rb and ^{96}Y were hence performed by applying the new technology of calorimetric low-temperature detectors (CLTDs) [24,25] at the LOHENGRIN mass spectrometer at the ILL in Grenoble, France. For determining isotopic fragment yields, a fairly universal method, namely, the passive absorber technique [26] exploiting the Z-dependent energy loss of fission fragments in an energy absorber, was applied. The CLTDs determine the particle energy by measuring
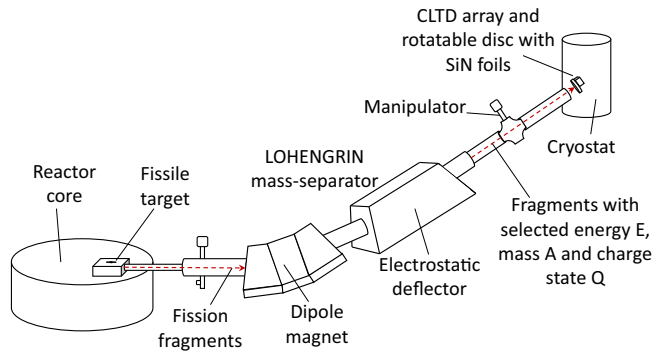
FIG. 1. Schematic of the experimental setup at the ILL reactor for isotopic yield measurements.
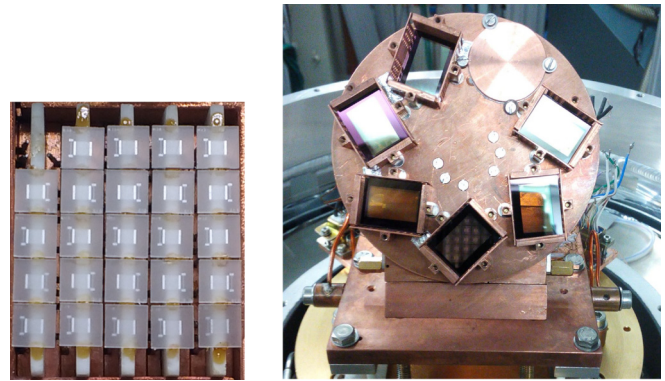

FIG. 2. Picture of the CLTD array (left). Picture of the rotatable disk with different SiN absorber foil stacks of different thicknesses mounted in front of the CLTD array (right).

the temperature rise due to thermalization of the particle's kinetic energy in the detector. Due to their principle of operation, which is independent of ionization processes, CLTDs provide very good energy linearity and resolution for the spectroscopy of heavy ions at low energies [24,25,27–36]. These advantages of CLTDs help in determining precise yields of ^{92}Rb and ^{96}Y for the three fissioning systems ^{235}U(n$_{th}$, f), ^{239}Pu(n$_{th}$, f), and ^{241}Pu(n$_{th}$, f) by an independent new method.

II. EXPERIMENTAL SETUP

The experiment for the isotopic yield determination of ^{92}Rb and ^{96}Y was performed at the LOHENGRIN fission-fragment spectrometer [37–39] at the high-flux reactor of the Institut Laue-Langevin in Grenoble. The schematic of the experimental setup is shown in Fig. 1. A fissile target [40] is placed in a vacuum tube protruding into the heavy water moderator of the reactor at about 50 cm distance from the core with a high thermal-neutron flux of about 5×10^{14} neutrons per second per cm^2. Recoiling fission fragments leave the target with a small energy loss as highly charged ions (typically with ionic charge states of 16 to 30). At 8 m from the target, the ionized fragments enter a horizontally deflecting homogeneous magnetic sector field separating fission fragments according to the ratio of momentum to ionic charge state, p/Q. Subsequently, the fragments pass through a vertically deflecting cylindrical condenser separating fragments according to the ratio of kinetic energy to ionic charge state, E/Q. The combination of magnetic and electric deflection represents a parabola mass spectrometer, resulting in a separation of the ionized fragments with respect to their mass over ionic charge state, A/Q, and velocity v, thus also defining a fixed ratio of kinetic energy to ionic charge state, E/Q. The fragments travel 23 m from the target to reach the exit flange of LOHENGRIN with a flight time of the order of 2 μs, allowing the determination of independent yields, as they reach the detector before undergoing β decay. Using the thin fissile targets with dimensions of the order of 4×0.5 cm^2, the mass resolution of the LOHENGRIN spectrometer is of the order of $A/\Delta A \approx 1000$, and the uncertainty in measuring the kinetic energy is <1%. At the LOHENGRIN exit, a manipulator is placed with different SiN absorber foil stacks, an aperture,

and, as complementary detector, a PIN diode which allows us to monitor the fragment beam without any absorber foil. The cryostat is connected to the beam line after the manipulator as shown in Fig. 1. Inside the cryostat, we have the CLTD array in front of which a rotatable disk is mounted with different thicknesses of SiN absorber foil stacks.

The detector array used in the present experiment consists of 24 independent detector pixels with transition-edge sensors (TESs) and has an active area of $\approx 15 \times 15$ mm^2 (Fig. 2). The individual pixels [29,30,34–36] consist of $3 \times 3 \times 0.43$ mm^3 sapphire absorbers onto which TES thermometers in the form of 10-nm-thick meander-shaped Al layers are deposited by photolithographic techniques. Each pixel is individually temperature regulated at the operational temperature of approximately 1.5 K via a 25-μm-thick gold layer deposited onto the pixel. For the readout, conventional pulse electronics consisting of low-noise pre-amplifiers and flash ADCs are used. The granular structure of the detector was chosen to keep the heat capacity of single pixels sufficiently small in order to provide high sensitivity. In a first attempt [31,34], SiN absorbers were mounted on a movable manipulator at a distance of 95 cm outside the cryostat, as shown in Fig. 1. This resulted in largely reduced counting efficiency due to small-angle scattering and increased the background by neighboring mass lines from the LOHENGRIN spectrometer. To counter these problems, the experimental setup was upgraded by installing a remotely controlled movable disk on which SiN absorber foil stacks of different thicknesses were mounted inside the cryostat, at a distance of a few millimeters to the CLTDs (Fig. 2). For rotating the disk, a piezo-driven rotary stepper positioner (ANR240/RES from Attocube) was used, which consists of a positioner with resistive encoder along with the controller ANC350. The device operates under vacuum and at temperatures as low as 10 mK and allows a reproducible positioning with an accuracy of 0.050 degrees ($\approx$30 μm for the current design). The SiN foil stacks mounted on this disk were 1, 4, 5, 6, 7 μm thick. In this way it was possible to optimize the absorber thickness with respect to the individual experimental conditions such as fragment mass and energy.

TABLE I. List of measurements for the different targets for determining isotopic yields for mass $A = 92$ and $A = 96$ at different LOHENGRIN energy and ionic charge state settings.

Target	$A = 92$	$A = 96$
^{235}U	E scans at $Q = 20$ and 25 for $E_L = 80, 88, 94, 100$, and 106 MeV. Q scans at $E_L = 94$ MeV for all Qs between 16 and 26.	E scans at $Q = 18$ and 21 for $E_L = 74, 80, 88, 94, 100, 102$, and 106 MeV. Q scans at $E_L = 84, 94$, and 102 MeV for all Qs between 16 and 26.
^{241}Pu	E scans at $Q = 21$ and 25 for $E_L = 86, 94, 100$, and 106 MeV.	E scans at $Q = 21$ for $E_L = 86, 94$, and 100 MeV as well as for $E_L = 94$ MeV at $Q = 18$.
^{239}Pu	E scans at $Q = 21$ for $E_L = 94, 100$, and 106 MeV. Q scans at $E_L = 100$ MeV for $Q = 17, 20, 21, 24$, and 25.	

III. MEASUREMENTS

Measurements were performed at different LOHENGRIN kinetic energy E_L and ionic charge state Q settings to determine independent and cumulative fission yields of ^{92}Rb and ^{96}Y for ^{235}U(n_{th}, f), and ^{239,241}Pu(n_{th}, f), respectively. Three fissile targets of highly enriched ^{235}U ($>99\%$ enrichment), ^{239}Pu (99.98%), and ^{241}Pu (71.1%) were used, all in the form of oxide deposits on thick titanium backings. For each target the effective area visible to the spectrometer was either defined by the area of the deposit, or constrained by a thick titanium diaphragm mounted on top of the target. The ^{235}U target had an effective area of 4×0.4 cm^2, was 128 μg cm^{-2} thick, and was covered by a sputtered tungsten layer of ≈ 100 nm to reduce losses by self-sputtering [40]. The ^{239}Pu target had an effective area of 4×0.3 cm^2, was 38 μg cm^{-2} thick, and was covered by a 0.25 μm Ni foil. The ^{241}Pu target had an effective area of 4×0.5 cm^2, was 24 μg cm^{-2} thick, and was covered by a 0.25 μm Ni foil. The ^{235}U and ^{239}Pu targets can be considered as "pure" since $\gg 99.9\%$ of the fission rate stems from the isotope of interest. For the ^{241}Pu target the remaining fraction is composed of nonfissile ^{240,242}Pu and 7.7% ^{241}Am produced by β^- decay of ^{241}Pu appearing since the Pu/Am separation before the target preparation. Due to its small fission cross section ^{241}Am(n, f) contributes only with 0.03% to the total fission rate, but $\approx 1.1\%$ of the fission rate is due to double neutron capture reactions ^{241}Am$(n, \gamma)^{242g}$Am(n, f) and ^{241}Am$(n, \gamma)^{242m}$Am(n, f), respectively. The reaction of interest ^{241}Pu(n, f) represents therefore 98.9% of the total fission rate. Fission fragments undergo energy loss in the target and in the cover of the target before they pass through the LOHENGRIN spectrometer. The original kinetic energies of the fission fragments are derived by calculating this energy loss in the target and its cover and adding it to the LOHENGRIN energy setting. The energy loss in the target and in the cover foil of the target was calculated for the different targets to be 4.9(1.8) MeV for ^{235}U(n_{th}, f), 6.7(1.9) MeV for ^{239}Pu(n_{th}, f), and 6.3(2.0) MeV for ^{241}Pu(n_{th}, f). A list of all measurements performed for determining the isotopic yields of mass $A = 92$ and mass $A = 96$ is presented in Table I. The complete set of data is published in Ref. [35] and original data files are available via Refs. [41,42]. In addition, for both masses ($A = 92$ and 96) and other masses used for normalization, measurements were performed with the complementary PIN-diode detector mounted on the manipulator at the exit of LOHENGRIN, as

shown in Fig. 1, to determine the energy and ionic charge state distributions of these masses in order to normalize the isotopic yields determined from the measurements with the CLTDs [34,35]. Also, the PIN-diode was used to perform the burn-up measurements for the target characteristics at LOHENGRIN.

IV. ANALYSIS

A. Data analysis

This section briefly discusses the procedure of determining fractional independent and cumulative yields from the CLTD measurements at the LOHENGRIN spectrometer. For details please refer to Ref. [35].

Cumulative fission yields of given isotopes, e.g., ^{92}Rb, can be obtained either by integral or differential measurements. Direct γ-ray spectrometry of nonseparated fission product samples is an integral method. Its main experimental limitation towards short-lived isotopes is the complexity of the γ-ray spectra to which the decays of hundreds of fission products contribute, each with several γ rays on average. Alternatively, differential measurements are performed after a suitable combination of A and/or Z separations. For example, a radiochemical separation could separate all isotopes of one element (fixed Z) which are then counted, while a mass separation separates all isobars with a given mass (fixed A). These separation methods can be used individually or in combination and are followed by a quantification method which is either nonselective (ion counting) or provides additional selectivity such as γ-ray spectrometry. Fast-fission-fragment beams can also be combined with nuclear-charge-sensitive detection methods, such as the $\Delta E / E$ method. The latter will provide fractional independent yields, which, multiplied by the respective mass yield, gives independent yields. Summation of the latter from low Z to higher Z (along the β^- decay paths) provides then the cumulative yields.[1]

The determination of independent or cumulative yields is therefore a separable problem where mass yields and fractional yields can be determined in different experiments and later combined. $A = 92$ and $A = 96$ belong to the light-fission-fragment peak and, for the common fissioning systems ^{235}U(n_{th}, f), ^{239}Pu(n_{th}, f), and ^{241}Pu(n_{th}, f), their

———

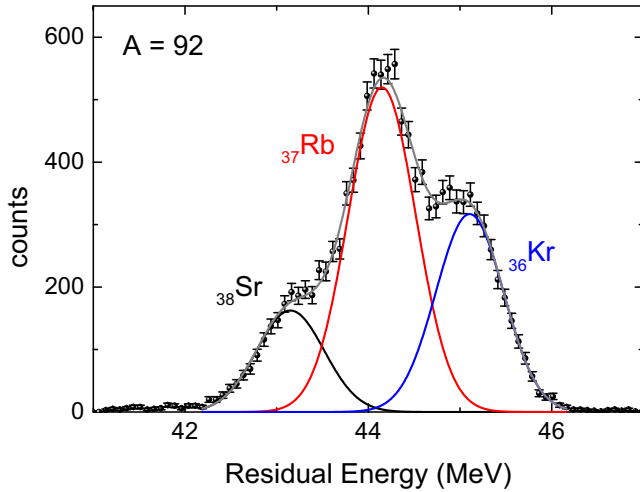[1] Mass-changing βn decays have negligible influence on the mass chains considered here.

FIG. 3. Example spectrum for isotopic yield determination for mass $A = 92$ at $E_L = 94$ MeV and for a 4-μm-thick SiN absorber foil fit with three Gaussian functions corresponding to contributions from different nuclear charges.

mass yields are relatively well known from numerous studies, e.g., Refs. [43–45]. However, data on the fractional yields are scarcer. The particular strengths of CLTDs are their high and reproducible isobaric resolution and, due to the granularity of the detector array, moreover, the perfect control of systematic effects such as subtle shifts of the beam position in the focal plane (see also Ref. [35]). Therefore, the present work focused on a new independent determination of fractional yields, while the mass yields were taken from literature and were complemented with consistency checks against other masses in the region with well-known yields.

Each measurement with a specific LOHENGRIN energy E_L and ionic charge state setting Q is analyzed by fitting Gaussian functions in the residual energy spectra in order to determine the relative isotopic yields. An example residual energy spectrum fit with three Gaussian functions is shown in Fig. 3 for mass 92. The relative isotopic yields are determined by the ratio of the area under the peaks (each corresponding to one nuclear charge) to the total area. Results for relative Z

yields for measurements at different LOHENGRIN energies and ionic charge states were convoluted with ionic charge state and kinetic-energy distributions of the respective masses measured with the PIN diode to determine the ionic charge state and kinetic-energy distributions of the corresponding nuclear charges. Examples for such distributions are displayed in Fig. 4. The complete data sets are presented in Ref. [35]. The ionic charge state and kinetic-energy distributions thus obtained are denoted by $Y(A, Z, Q_i, E_j)$. The fractional isotopic yields which correspond to the integral over the ionic charge state and the kinetic-energy distributions are given by evaluating the following sum of integrals:

$$Y(A, Z) = \sum_i \int_E Y(A, Z, Q_i, E) dE. \quad (1)$$

It is a time-consuming procedure to perform measurements for all possible ionic charge state and kinetic-energy settings at LOHENGRIN; therefore, a simpler approach [46,47] to estimate the yields was applied, which is given by

$$Y(A, Z) = \frac{\int_E Y(A, Z, \bar{Q}, E) dE \sum_i (A, Z, \bar{E}, Q_i)}{Y(A, Z, \bar{Q}, \bar{E})}. \quad (2)$$

With this procedure, yields can be determined by measuring a single ionic charge state distribution at a mean kinetic energy $\bar{E}$ and a single kinetic-energy distribution at a mean ionic charge state $\bar{Q}$. Measured kinetic-energy distributions are fit with exponentially modified Gaussian functions, as shown in Fig. 4, and both the quantities $\int_E Y(A, Z, \bar{Q}, E) dE$ and $\sum_i Y(A, Z, \bar{E}, Q_i)$ are determined from the values of the Gaussian integral and sum, respectively. Finally, to determine the independent yields which correspond to the yields directly from fission, fractional isotopic yields were multiplied by the mass yields determined with the PIN-diode normalized to Lisman *et al.* [43]. The mass yields determined for $A = 90$, 95 and 99 from PIN-diode measurements, normalized to the mass yields for $A = 92$ and $A = 96$, are fully consistent with the respective values from Lisman *et al.* [43] and the JEFF-3.3 data library [48]. Masses 90, 95, and 99 were chosen because the cumulative fission yields of ^{90}Sr, ^{95}Zr, and ^{99}Mo cover >99.9% of the respective mass yields, and these cumulative

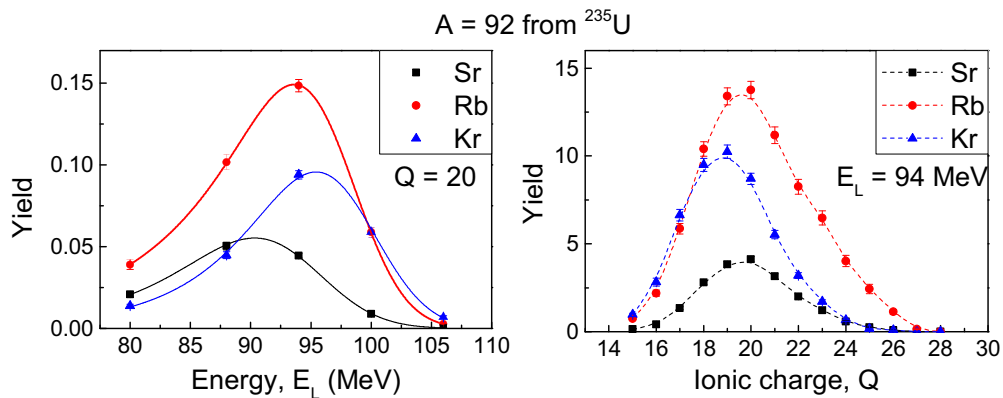
FIG. 4. Examples for kinetic energy (left) and ionic charge state distributions (right) of isotopic yields of mass $A = 92$ for ^{235}U(n_{th}, f). Solid lines on the left are exponentially modified Gaussian fits and dotted lines on the right are used to connect data points to follow the trend.

yields are accurately known also from radiochemical measurements.

We note that ^{96}Y has two beta-decaying states, the 0^- ground state ^{96g}Y($T_{1/2} = 5.34$ s) and the 8^+ isomeric state ^{96m}Y($T_{1/2} = 9.6$ s). Both are populated in nuclear fission, but only the beta decay of ^{96g}Y contributes significantly to antineutrino spectra above 4 MeV while the beta decay of ^{96m}Y feeds higher-lying high-spin levels in ^{96}Zr, which increases the fraction of the Q value released as γ rays at the expense of energy released by betas and antineutrinos. The method used in the present experiment is only sensitive to isotopes but not to isomers. Thus we report the isotopic yield ^{96}Y which represents the sum of the yields of both beta-decaying isomers ^{96g}Y and ^{96m}Y. An additional measurement with an independent method (γ-ray spectrometry at LOHENGRIN) is required to obtain the isomeric ratio ^{96g}Y / ^{96m}Y and thus transform the ^{96}Y sum yield reported here into the individual yield of ^{96g}Y relevant for the antineutrino spectra. Since ^{96g}Y decays dominantly to the ground state of ^{96}Zr or to the first-excited 0^+ state, only few γ rays accompany this decay and their intensities carry large uncertainties. Thus, a more precise value for the individual ^{96g}Y yield can be obtained by comparing the ^{96m}Y and ^{96}Sr yields, which both emit intense γ rays with well-known intensities, then subtract the so-determined ^{96m}Y yield from the total $^{96g+m}$Y yield. For this purpose we provide also the newly measured independent and cumulative ^{96}Sr yield and the $^{96g+m}$Y / ^{96}Sr yield ratio, respectively, where some experimental uncertainties cancel.

B. Corrections and error analysis

The corrections applied in the procedure of yield determination are discussed below (for details see Ref. [35]):

(1) Energy acceptance of the LOHENGRIN spectrometer: The relation between kinetic energy E_L of the fragments measured by LOHENGRIN and the LOHENGRIN energy acceptance ΔE which is, due to the small acceptance ($\Delta E_L \ll E_L$), given by the linear equation $\frac{\Delta E_L}{E_L} = \frac{\Delta x}{D_E}$, where $D_E = 7.2$ m is the energy dispersion of the spectrometer. The acceptance Δx is given by the detector size, so the ratio $\Delta x/D_E$ is constant. The accepted energy range is therefore proportional to the chosen energy. To correct for this effect, all count rates are divided by the energy set at the LOHENGRIN spectrometer for normalization.

(2) Target burn-up: When placed in a high neutron flux, the fission rate of the target decreases with time due to the loss of target material [40]. To account for the target burn-up, the decrease in fission rate was monitored regularly (once to twice a day) by measuring a reference mass. The target burn-up curve thus obtained is described with an exponential decay curve and corresponding corrections were applied in the yield calculations.

The various sources of errors identified are discussed below (for details see Ref. [35]):

(1) Statistical uncertainties: The statistical uncertainty as well as errors corresponding to the Gaussian fit of the residual energy spectra measured by the CLTDs was determined by using OriginLab software. Additionally, a statistical effect is caused by the thermal-neutron-flux stability. An upper limit of possible local fluctuations can be determined by measuring a reference mass frequently, and, based on the reproducibility of these measurements, the variations in the yields are estimated to be less than 0.6% based on previous work [46].

(2) Systematic uncertainties: The approximation given by Eq. (2) is rigorous only when Q and E are uncorrelated, which is not strictly the case. The error introduced due to this assumption can be determined by comparing the results on yields with measurements for all ionic charge state and kinetic-energy combinations with respect to the result from measurements for only one kinetic-energy distribution at a mean ionic charge state, and one ionic charge state distribution at a mean energy. This leads to an uncertainty of less than 1.3% [35,49].

(3) Nanosecond isomers: Electromagnetic spectrometers can provide precise fission yields down to very low relative abundances (at LOHENGRIN $\approx 10^{-10}$ per fission [50]), but the implicit sensitivity to the ionic charge state distribution of the fission fragments may induce artifacts in certain cases. Usually the ionic charge state distribution observed at LOHENGRIN is the result of electron stripping and electron capture when the fast ions traverse the target cover, reaching a statistical distribution around an equilibrium charge state. For fission fragments with kinetic energies of 0.5–1 MeV/nucleon, the ionic charge state distribution happens then to be nearly Gaussian [51,52]. However, fission populates the fragments with a certain excitation energy and spin. The high spin levels usually decay quickly via a γ-ray cascade to the ground state or a longer-lived isomer. In certain cases, isomeric states exist in the decay cascade where γ-ray emission is strongly hindered and the decay proceeds via internal conversion, i.e., emission of conversion electrons followed by a cascade of Auger electrons. When the isomeric state has a lifetime of the order of nanoseconds, the change of ionic charge state happens after leaving the target cover, but before entering the magnetic deflection. Consequently, a perturbed ionic charge state distribution is observed with a second component at higher charge states, corresponding to the relative isomeric yield of the nanosecond-isomer times $\alpha/(1 + \alpha)$, where α is the conversion coefficient of its decay [46,53,54]. ^{92}Rb has a series of three nanosecond isomers with partially converted $M1$ and $E2$ transitions in its yrast cascade [55] which will shift part of the ionic charge state distribution to higher Q. The corresponding asymmetry observed in the Q distribution is shown in Fig. 4.

(4) Normalization errors: To determine the independent nuclear charge yields, we multiply the fractional

TABLE II. Fractional independent yield per $A = 92$ (%), Y_{frac} and independent yield per fission, Y_{ind} for mass $A = 92$ for thermal-neutron-induced fission of the three targets ^{235}U, ^{239}Pu, and ^{241}Pu. The last row presents the cumulative yield for ^{92}Rb for the three targets.

Isotope	^{235}U(n_{th}, f)		^{239}Pu(n_{th}, f)		^{241}Pu(n_{th}, f)	
	$Y_{frac}(\%)$	Y_{ind}	$Y_{frac}(\%)$	Y_{ind}	$Y_{frac}(\%)$	Y_{ind}
^{92}Br	<0.5	<0.0003	<0.5	<0.0001	<0.5	<0.0001
^{92}Kr	32.0(18)	0.0190(11)	11.6(16)	0.0035(5)	17.2(12)	0.0038(3)
^{92}Rb	51.7(31)	0.0308(18)	49.7(47)	0.0150(14)	62.5(30)	0.0139(8)
^{92}Sr	15.6(11)	0.0093(7)	37.9(53)	0.0115(16)	19.6(26)	0.0044(6)
^{92}Y	<1	<0.0006	<1	<0.0003	<1	<0.0002
Cum. ^{92}Rb		0.0499(8)		0.0186(15)		0.0178(8)

nuclear charge yields, determined from the CLTD measurements, with the respective mass yields derived from the PIN-diode with respect to the known mass yields [43], and their respective uncertainties are incorporated.

The total uncertainty Δ_{tot} is then calculated as follows:

$$\Delta_{tot} = \sqrt{(\Delta_{statistical} + \Delta_{systematic})^2 + \Delta_{normalization}^2}. \quad (3)$$

V. RESULTS AND DISCUSSION

A. Results from the present experiment

The fractional and independent isotopic yields for mass $A = 92$ for the three targets are listed in Table II. The last row of the table presents the cumulative yields of ^{92}Rb for the three targets. Table III lists the fractional and independent isotopic yields for mass 96 for thermal-neutron-induced fission of the two targets ^{235}U and ^{241}Pu. Also presented in this table are the cumulative yield of ^{96}Sr and the $^{96g+m}$Y / ^{96}Sr yield ratio for a precise yield determination of ^{96g}Y, as discussed in Sec. IV A.

In all the measured spectra of mass 92, three isobars were identified as ^{92}Kr, ^{92}Rb, and ^{92}Sr, while only upper limits were found for isobars with other Z, namely <0.5% for ^{92}Br and <1% for ^{92}Y. Correspondingly, for mass 96, four isobars were identified and upper limits were derived for the nonobserved isobars <0.6% for ^{96}Kr and <1.6% for ^{96}Nb. These

TABLE III. Fractional independent yield per $A = 96$ (%), Y_{frac} and independent yield per fission, Y_{ind} for mass $A = 96$ for the two fissioning systems ^{235}U(n_{th}, f) and ^{241}Pu(n_{th}, f). The last two rows present the cumulative yield for ^{96}Sr and the ratio of the independent yield of $^{96g+m}$Y to the cumulative yield of ^{96}Sr for the two targets.

Isotope	^{235}U(n_{th}, f)		^{241}Pu(n_{th}, f)	
	$Y_{frac}(\%)$	Y_{ind}	$Y_{frac}(\%)$	Y_{ind}
^{96}Kr	<0.6	<0.0004	<0.6	<0.0003
^{96}Rb	4.2(3)	0.0026(2)	3.8(4)	0.0016(2)
^{96}Sr	54.4(21)	0.0339(13)	57.9(29)	0.0251(14)
^{96}Y	34.1(14)	0.0212(9)	32.9(30)	0.0143(13)
^{96}Zr	6.3(5)	0.0039(3)	4.4(9)	0.0019(4)
^{96}Nb	<1.6	<0.001	<1.6	<0.0007
Cum. ^{96}Sr		0.0366(11)		0.0268(16)
$^{96g+m}$Y / ^{96}Sr		0.579(29)		0.532(55)

limits are accounted for in the calculation of cumulative yields by symmetrizing the upper limits. The cumulative yield of ^{92}Rb for ^{235}U(n_{th}, f) was also determined in the first attempt [31,34] of isotopic yield determination with the CLTDs, with the reported value of 0.0471 ± 0.0037 which is in good agreement with the present result.

The first generation of fractional fission yield measurements at LOHENGRIN had been performed with one or few Q and E settings close to the peak of the distributions [65–67]. As evident from our Fig. 4 and as discussed in detail by Wohlfarth *et al.* [53] for some nuclides with particular ionic charge state distributions (e.g., ^{92}Rb), measurements at the peak of the distribution are not fully representative for the average fractional yield in fission. Later measurements took this observation into account and covered a wider Q range [63,64]. Another difference to previous LOHENGRIN measurements is the target coverage. Experiments that measured the "unperturbed" kinetic-energy distributions in the same run prefer minimum-energy corrections and would use uncovered targets. However, such targets are also prone to very rapid and less regular burn-up and their ionic charge state distributions may evolve significantly during burn-up [63]. In contrast to prior single-detector measurements, the use of a detector array with 24 independent pixels in the present experiment allowed us to cross-check and validate the individual spectra and eliminate artifacts from neighboring A/Q ratios that may spill in at the edge of the mass-defining slit (for details see Ref. [35]).

Figure 5 compares the cumulative yields for ^{92}Rb determined in the present work with values reported in nuclear data libraries JENDL-4.0 [56], JEFF-3.3 [48], and ENDF/B-VIII.0 [57], the GEF Code GEFY-6.2 [58,59], and the experimental values from Refs. [21,60–64]. Norris *et al.* [60] and Schillebeeckx *et al.* [62] determined fractional independent yields. For the purpose of plotting we summed these values and multiplied them with the mass yield from Lisman *et al.* [43]. For the most important fissioning system ^{235}U(n_{th}, f), the newly measured value is in good agreement with nuclear data libraries and the GEF code, and with most previous measurements performed with different techniques and instruments. However, a clear disagreement is observed for the ^{92}Rb cumulative yield reported by Tipnis *et al.* [21]. This issue will be discussed in the next section. It is noteworthy that, for the fissioning systems ^{239}Pu(n_{th}, f) and ^{241}Pu(n_{th}, f), our cumulative fission yields for ^{92}Sr and ^{92}Y respectively match well those determined by Dickens *et al.* [68,69] gamma-spectrometrically, i.e., with a method not relying on
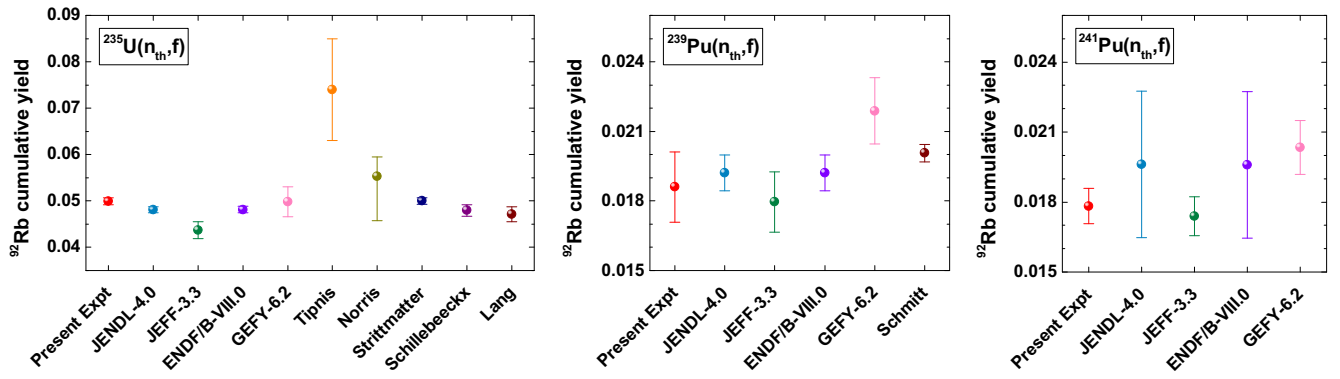
FIG. 5. Cumulative yields of ^{92}Rb measured for the three targets ^{235}U(n_{th}, f), ^{239}Pu(n_{th}, f), and ^{241}Pu(n_{th}, f) are shown in red. The present results are compared with the nuclear data libraries JENDL-4.0 [56], JEFF-3.3 [48], and ENDF/B-VIII.0 [57], the GEF Code GEFY-6.2 [58,59], and the experimental values of Tipnis *et al.* [21], Norris *et al.* [60], Strittmatter [61], Schillebeeckx *et al.* [62], and Lang *et al.* [63] for ^{235}U, and Schmitt *et al.* [64] for ^{239}Pu, respectively.

normalization with mass yields. Moreover, the independent fission yields given by the GEF code match also remarkably well with those measured for $A = 96$, see Fig. 6.

B. The puzzle of the UML measurement

Tipnis *et al.* [21] performed a detailed study of thermal-neutron-induced fission yields at the University of Massachusetts, Lowell (UML) Van de Graaff facility by coupling a ^{235}U target via a gas jet to a beta-γ-ray spectroscopy setup. They derived independent and cumulative fission yields for 41 different isotopes and isomers from ^{89}Rb to ^{147}La. While most values do agree within uncertainties with the ENDF/B-VI evaluation and a previous measurement by Rudstam *et al.* [70], a few major discrepancies were observed, notably for ^{92}Rb. They explain in the text that γ-ray intensities from Rudstam *et al.* [70] were used instead of those from the then latest Nuclear Data Sheets evaluation [71]. However, the numeric values given in Table II of the UML paper [21] (3.56% for 815 keV, 0.65% for 1712 keV, 1.07% for 2821 keV, no uncertainties given) differ considerably from the intensities quoted in Ref. [70] [4.0(3)% for 815 keV, 0.53(4)% for 1712 keV, 0.75(6)% for 2821 keV], which in turn differ from the currently adopted values [55] [3.2(4)% for 815 keV, 0.42(6)% for 1712 keV, 0.60(9)% for 2821 keV]. The intensities quoted

by UML are thus between the value of Rudstam *et al.* and the currently adopted value for the 815 keV line, but considerably higher than the other references for the 1712 and 2821 keV lines. It is not traceable how much statistical weight each of the three γ lines contributes to the finally derived yield value, but it can be assumed that the higher-energy lines with lower γ-ray intensities and lower Ge detector efficiency contribute relatively little weight compared with the 815 keV line. Even if they contributed more, this could not explain an upward bias to the derived yield because the latter is obtained by dividing experimental counts by the γ-line intensity per decay, i.e., a higher value of the latter would reduce the yield, not increase it. If the ^{92}Rb yield was derived exclusively or dominantly from the intensity of the 815 keV line, then one would expect a slight [(12(8)%] overestimation with respect to Rudstam *et al.* or a slight [10(11)%] underestimation with respect to present γ-ray intensities, but definitely not a factor-of-two deviation. We can conclude that the UML data point cannot be reconciled with other measurements by a simple renormalization with different γ-ray intensities.

In addition, specifically for rubidium isotopes, five data sets are available from measurements at isotope separation online (ISOL) separators where fission products are thermally released from thick, heated ^{235}UC$_x$/graphite targets, then the alkali elements are selectively surface ionized on a hot metal
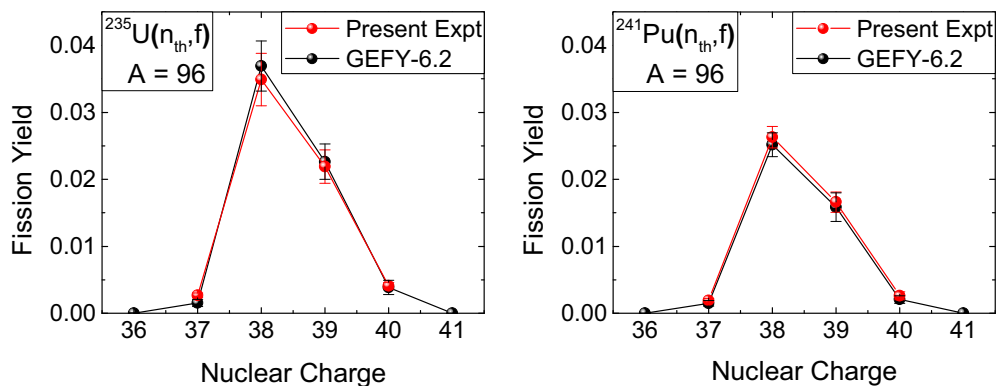

FIG. 6. Independent isotopic yield results from the present experiment for mass $A = 96$ in comparison with the GEF calculation [58].
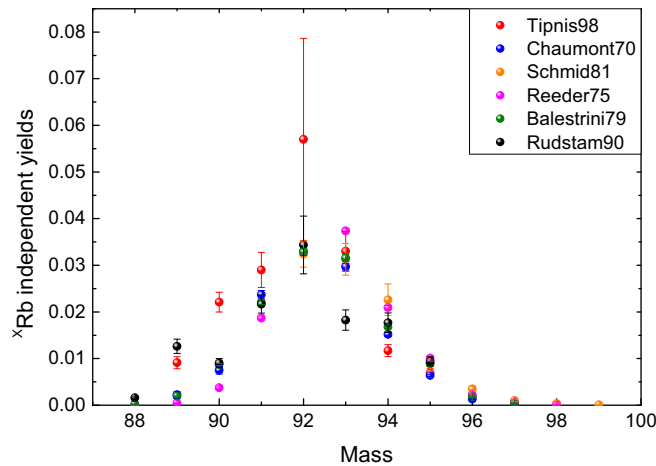
FIG. 7. Independent yields of ^{X}Rb isotopes from the UML measurement (Tipnis98) [21] versus measurements at ISOL facilities [70,72–75]. For the purpose of comparison, the relative yields of Reeder75 [73] were normalized at $A = 92$ to the yields given by Chaumont70 [72].

(Ta or Re) surface. Chaumont used a mass separator at an external neutron beam of the EL3 reactor in Saclay, France and quantified the ion beams by direct ion counting with a secondary electron multiplier [72]. Reeder *et al.* used the SOLAR separator at Washington State University, USA and counted ions by a secondary electron multiplier [73]. A pulsed release technique allowed us to distinguish between cumulative and independent yields. Also, Balestrini *et al.* used a pulsed release technique at the OSTIS separator at ILL, again with direct ion counting [74]. Shmid *et al.* used beams from the SOLIS separator at Soreq combined with beta counting [75]. Finally, Rudstam *et al.* analyzed the beams separated with the OSIRIS separator in Studsvik by γ-ray spectrometry and, for the most-neutron-rich isotopes, delayed neutron detection, respectively [70,76].

Strictly speaking, yields are determined from ISOL targets only truly "independent" for shielded isotopes. For other cases that are part of a decay chain, the radioactive precursors may feed the nuclide of interest by in-target decay that is more or less pronounced, depending on the ratio of release time versus half-life of the respective precursor isotope. Thus, measured yields of such nuclides may take values between the independent and the cumulative yield. The pulsed release technique allows a better discrimination. With different ionization methods, Rudstam *et al.* also studied the yields and release of the krypton and bromine precursors to correct for their contribution [77], while the other works only observed rubidium. Thus, the not-directly-measured Br and Kr diffusion sets a limit on the accuracy of Rb yields close to stability. The ionization efficiencies were not determined directly, thus the observed ion rates had to be normalized, for one or several masses, to literature values. Therefore, none of these yield measurements with the ISOL method is a completely independent measurement, but clearly the relative yields along the isotope chain allow a direct comparison with the UML measurement. As shown in Fig. 7, most values stay

relatively well grouped with differences either due to different detection methods or incomplete resolution of the in-target decay issue. However, the UML measurement shows a clearly different structure highlighting again the ^{92}Rb point as an outlier, even if it is less pronounced.

C. The problem of the ^{92}Rb → ^{92}Sr ground-state decay

The example of the UML measurement demonstrates the intrinsic problem of determining fission yields by γ-ray spectrometry. The so-derived fission yields are only as accurate as the knowledge of the decay properties exploited in the analysis, in particular the γ-ray intensities. Specifically, fission products that are dominantly beta decaying to the ground state will have small γ-ray intensities that are often known less reliably. This effect is particularly pronounced for ^{92}Rb and ^{96g}Y, the two fission products which are dominating the high-energy β spectra and thus the antineutrino spectra of fission products. This is directly linked to the dominant ground-state transition, which leads to a large fraction of the decay Q value going into β and antineutrino energy instead of γ rays. The ground state of ^{92}Rb is a 0^- level which β decays dominantly to the 0^+ ground state of ^{92}Sr, without accompanying γ-ray emission. Smaller β decay branches to higher-lying levels (mainly allowed transitions to levels with spin 1 or 0) will either decay via the first-excited 2^+ level at 815 keV, or directly to the ground state. Due to the high Q value of 8095(6) keV for the β^- decay of ^{92}Rb, in principle excited levels up to ≈ 8 MeV can be populated in ^{92}Sr. This leads to the well-known pandemonium problem where weak high-energy γ-ray transitions may even escape detection by large Ge detectors. According to the latest ENSDF evaluation [55], the branching for the ^{92}Rb β^- decay to the ^{92}Sr ground-state decay is 95.2(7)%, while in 3.2(4)% of the decays a 815 keV γ ray is emitted, as determined by Lhersonneau *et al.* [78]. In other words, $\varepsilon = 4.8(7)\%$ of the decays lead to excited states and 67(8)% of these decays will proceed through the 2^+ level to the ground state. However, the ground-state population $(1 - \varepsilon)$ has seen some variation over time: 94(+6/−20)% [79], 51(18)% [71,80], $\approx$90% [21], 87.5(25)% [18], and 91(3)% [19]. The weighted average of the latter two values from recent total absorption spectroscopy (TAS) measurements is 89(2)%, i.e., $\varepsilon = 11(2)\%$. The ^{92}Rb decay dominates by far the antineutrino spectra above 7 MeV ($\approx$38% contribution in a standard PWR spectrum [18] based on JEFF-3.3 yields [10]), and this contribution is obviously completely dominated by the ground-state branch. Thus, the quantitative prediction of this contribution to the high-energy antineutrino flux with the summation method has about 2% uncertainty from the decay branch plus the uncertainty of the ^{92}Rb cumulative yield which is 4.3% for our value for ^{235}U$(n_{\text{th}}, \text{f})$. However, a γ-ray spectrometric yield measurement would divide the observed γ-ray intensity by $\varepsilon \times 0.67$ to obtain the yield. This induces an uncertainty of at least $\delta(\varepsilon)/\varepsilon = 2/11 = 18\%$ (considering the ratio 2/3 as fixed) or larger (when yet-unobserved pandemonium decays proceed with a different fraction than 2/3 815 keV γ rays to the ground state), even if the experimental statistical and systematic errors were negligible.

VI. CONCLUSIONS

The cumulative yields for ^{92}Rb were determined for ^{235}U(n_{th}, f), ^{239}Pu(n_{th}, f), and ^{241}Pu(n_{th}, f) and the independent yields for ^{96}Y were determined for ^{235}U(n_{th}, f) and ^{241}Pu(n_{th}, f) from an independent measurement by using the novel technology of calorimetric low-temperature detectors at the LOHENGRIN spectrometer at the ILL reactor. The ^{92}Rb and ^{96}Y yields are in good agreement with the nuclear data libraries like JENDL-4.0 [56], JEFF-3.3 [48], and ENDF/B-VIII.0 [57], the GEF code GEFY-6.2 [58,59], and prior experimental values. However, the measurement by Tipnis *et al.* [21] for ^{235}U(n_{th}, f) reported a 1.5 times higher cumulative yield as compared with the yield determined in the present work. We conclude that the value of Tipnis *et al.* has to be considered as a clear outlier. Computing the reactor antineutrino anomaly based on the yields reported by Tipnis *et al.* for ^{92}Rb, the high-energy part of the antineutrino spectra would further increase the anomaly by 8%. With the new measurement in the present work, we could confirm that the yields reported by the data libraries are indeed more reliable. We may conclude that independently of the UML measurement which may have suffered from additional problems, γ-ray spectrometric yield determinations may have intrinsic shortcomings, in particular for those fission products which are most relevant for the high-energy part of reactor antineutrino spectra. Yields determined by direct ion counting are clearly preferred for these cases.

[1] G. Mention, M. Fechner, T. Lasserre, T. A. Mueller, D. Lhuillier, M. Cribier, and A. Letourneau, Phys. Rev. D **83**, 073006 (2011).

[2] K. Schreckenbach *et al.*, Phys. Lett. B **99**, 251 (1981).

[3] F. von Feilitzsch *et al.*, Phys. Lett. B **118**, 162 (1982).

[4] K. Schreckenbach *et al.*, Phys. Lett. B **160**, 325 (1985).

[5] A. Hahn *et al.*, Phys. Lett. B **218**, 365 (1989).

[6] J. H. Choi *et al.*, Phys. Rev. Lett. **116**, 211801 (2016).

[7] F. P. An *et al.*, Phys. Rev. Lett. **116**, 061801 (2016).

[8] Y. Abe *et al.*, J. High Energy Phys. 01 (2016) 163.

[9] B. R. Davis, P. Vogel, F. M. Mann, and R. E. Schenter, Phys. Rev. C **19**, 2259 (1979).

[10] M. Fallot *et al.*, Phys. Rev. Lett. **109**, 202504 (2012).

[11] A. A. Sonzogni, T. D. Johnson, and E. A. McCutchan, Phys. Rev. C **91**, 011301(R) (2015).

[12] D. A. Dwyer and T. J. Langford, Phys. Rev. Lett. **114**, 012502 (2015).

[13] H. Almazán *et al.*, Phys. Rev. Lett. **121**, 161801 (2018).

[14] J. Ashenfelter *et al.*, Phys. Rev. Lett. **121**, 251802 (2018).

[15] G. Bak *et al.*, Phys. Rev. Lett. **121**, 201801 (2018).

[16] D. Adey *et al.*, Phys. Rev. Lett. **121**, 241805 (2018).

[17] Y. J. Ko *et al.*, Phys. Rev. Lett. **118**, 121802 (2017).

[18] A.-A. Zakari-Issoufou *et al.*, Phys. Rev. Lett. **115**, 102503 (2015).

[19] B. C. Rasco *et al.*, Phys. Rev. Lett. **117**, 092501 (2016).

[20] A. Fijałkowska *et al.*, Phys. Rev. Lett. **119**, 052503 (2017).

[21] S. V. Tipnis, J. M. Campbell, G. P. Couchell, S. Li, H. V. Nguyen, D. J. Pullen, W. A. Schier, E. H. Seabury, and T. R. England, Phys. Rev. C **58**, 905 (1998).

[22] A. A. Sonzogni, E. A. McCutchan, T. D. Johnson, and P. Dimitriou, Phys. Rev. Lett. **116**, 132502 (2016).

[23] Y. Abe *et al.*, Phys. Rev. Lett. **108**, 131801 (2012).

[24] P. Egelhof, in *Advances in Solid State Physics* (Springer, Berlin, Heidelberg, 1999), Vol. 39, p. 61.

[25] P. Egelhof and S. Kraft-Bermuth, in *Topics in Applied Physics: Cryogenic Particle Detection* (Springer, 2005), Vol. 99, p. 469.

[26] U. Quade *et al.*, Nucl. Instrum. Methods **164**, 435 (1979).

[27] S. Kraft-Bermuth, Ph.D. thesis, JGU Mainz, 2004 (unpublished).

[28] S. Kraft-Bermuth *et al.*, Rev. Sci. Instrum. **80**, 103304 (2009).

[29] A. Echler *et al.*, J. Low Temp. Phys. **176**, 1033 (2014).

[30] A. Echler *et al.*, Nucl. Instrum. Methods Phys. Res., Sect. B **391**, 38 (2017).

[31] P. Grabitz *et al.*, J. Low Temp. Phys. **184**, 944 (2016).

[32] S. Dubey *et al.*, J. Low Temp. Phys. **193**, 1257 (2018).

[33] S. Dubey *et al.*, EPJ Web Conf. **193**, 04002 (2018).

[34] P. Grabitz, Ph.D. thesis, JGU Mainz, 2019 (unpublished).

[35] S. Dubey, Ph.D. thesis, JGU Mainz, 2019 (unpublished).

[36] A. Echler, Ph.D. thesis, JGU Mainz, 2013 (unpublished).

[37] E. Moll *et al.*, Nucl. Instrum. Methods **123**, 615 (1975).

[38] P. Armbruster *et al.*, Nucl. Instrum. Methods **139**, 213 (1976).

[39] E. Moll *et al.*, Kerntechnik und Atompraxis **19**, 374 (1977).

[40] U. Köster *et al.*, Nucl. Instrum. Methods Phys. Res., Sect. A **613**, 363 (2010).

[41] P. Egelhof *et al.*, Institut Laue-Langevin (ILL) (2015), doi: 10.5291/ILL-DATA.3-01-637.

[42] P. Egelhof *et al.*, Institut Laue-Langevin (ILL) (2016), doi: 10.5291/ILL-DATA.3-01-646.

[43] F. L. Lisman *et al.*, Nucl. Sci. Eng. (La Grange Park, IL, US) **42**, 191 (1970).

[44] W. J. Maeck *et al.*, Allied Chem. Corp., Idaho Chem. Programs **1142** (1978).

[45] W. J. Maeck *et al.*, Exxon Nucl. Idaho Company Report ENICO-1001 (1979).

[46] A. Bail, O. Serot, L. Mathieu, O. Litaize, T. Materna, U. Koster, H. Faust, A. Letourneau, and S. Panebianco, Phys. Rev. C **84**, 034605 (2011).

[47] Y. K. Gupta *et al.*, Phys. Rev. C **96**, 014608 (2017).

[48] A. J. M. Plompen *et al.*, Eur. Phys. J. A **56**, 181 (2020).

[49] A. Bail, Ph.D. thesis, University of Bordeaux, 2009 (unpublished).

[50] U. Köster *et al.*, Nucl. Phys. A **652**, 371 (1999).

[51] H. D. Betz, Rev. Mod. Phys. **44**, 465 (1972).

[52] H. D. Betz, in *Methods in Experimental Physics* (Elsevier, 1980), p. 73.

[53] H. Wohlfarth *et al.*, Z. Phys. A: At. Nucl. **287**, 153 (1978).

[54] B. Q. Lee, Ph.D. thesis, Australian National University, 2017 (unpublished).

[55] C. M. Baglin, Nucl. Data Sheets **113**, 2187 (2012).

[56] K. Shibata *et al.*, J. Nucl. Sci. Technol. (Abingdon, UK) **48**, 1 (2011).

[57] D. A. Brown *et al.*, Nucl. Data Sheets **148**, 1 (2018).

[58] Gef code, version 2018/1.1, http://www.khs-erzhausen.de/GEF-2018-1-1.html (2018).

[59] K.-H. Schmidt *et al.*, Nucl. Data Sheets **131**, 107 (2016).

[60] A. E. Norris and A. C. Wahl, Phys. Rev. **146**, 926 (1966).

[61] R. B. Strittmatter, Ph.D. thesis, University of Illinois, 1978 (unpublished).

[62] P. Schillebeeckx *et al.*, Nucl. Phys. A **580**, 15 (1994).

[63] W. Lang *et al.*, Nucl. Phys. A **345**, 34 (1980).

[64] C. Schmitt *et al.*, Nucl. Phys. A **430**, 21 (1984).

[65] G. Siegert *et al.*, Phys. Lett. B **53**, 45 (1974).

[66] H. G. Clerc *et al.*, Z. Phys. A: At. Nucl. **274**, 203 (1975).

[67] G. Siegert *et al.*, Phys. Rev. C **14**, 1864 (1976).

[68] J. K. Dickens and J. W. McConnell, Nucl. Sci. Eng. (La Grange Park, IL, US) **73**, 42 (1980).

[69] J. K. Dickens, Nucl. Sci. Eng. (La Grange Park, IL, US) **70**, 177 (1979).

[70] G. Rudstam *et al.*, Radiochim. Acta **49**, 155 (1990).

[71] C. M. Baglin, Nucl. Data Sheets **66**, 347 (2000).

[72] J. Chaumont, Ph.D. thesis, Université Paris Sud, 1970 (unpublished).

[73] P. Reeder *et al.*, Proc. Nucl. Cross Sections and Technol. **1**, 401 (1975).

[74] S. J. Balestrini, R. Decker, H. Wollnik, K. D. Wunsch, G. Jung, E. Koglin, and G. Siegert, Phys. Rev. C **20**, 2244 (1979).

[75] M. Shmid *et al.*, J. Inorg. Nucl. Chem. **43**, 867 (1981).

[76] G. Rudstam *et al.*, Studsvik Sci. Res. Lab. Rep. (1985).

[77] G. Rudstam *et al.*, Nucl. Instrum. Methods Phys. Res., Sect. A **256**, 465 (1987).

[78] G. Lhersonneau *et al.*, Phys. Rev. C **74**, 017308 (2006).

[79] R. Olson *et al.*, Phys. Rev. C **5**, 2095 (1972).

[80] C. M. Baglin, Nucl. Data Sheets **91**, 423 (2000).